

# ChemComm

Accepted Manuscript



This article can be cited before page numbers have been issued, to do this please use: Z. Huang, Q. Yao, J. Chen and Y. Gao, *Chem. Commun.*, 2018, DOI: 10.1039/C8CC02648C.



This is an Accepted Manuscript, which has been through the Royal Society of Chemistry peer review process and has been accepted for publication.

Accepted Manuscripts are published online shortly after acceptance, before technical editing, formatting and proof reading. Using this free service, authors can make their results available to the community, in citable form, before we publish the edited article. We will replace this Accepted Manuscript with the edited and formatted Advance Article as soon as it is available.

You can find more information about Accepted Manuscripts in the [author guidelines](#).

Please note that technical editing may introduce minor changes to the text and/or graphics, which may alter content. The journal's standard [Terms & Conditions](#) and the ethical guidelines, outlined in our [author and reviewer resource centre](#), still apply. In no event shall the Royal Society of Chemistry be held responsible for any errors or omissions in this Accepted Manuscript or any consequences arising from the use of any information it contains.

Journal Name

COMMUNICATION

## Redox Supramolecular Self-Assemblies Nonlinearly Enhance Fluorescence to Identify Cancer Cells

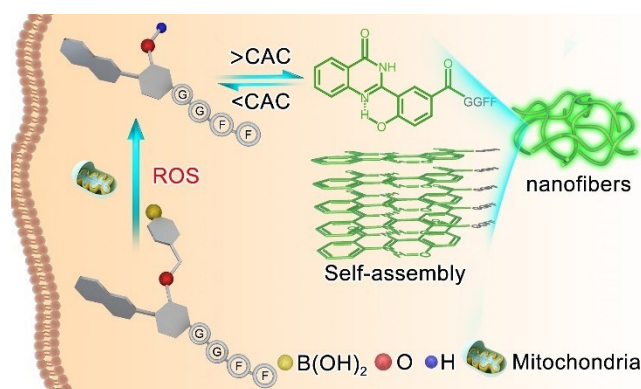
Zhentao Huang,<sup>1</sup> Qingxin Yao,<sup>1</sup> Jiali Chen<sup>1</sup> and Yuan Gao<sup>1,\*</sup>Received 00th January 20xx,  
Accepted 00th January 20xx

DOI: 10.1039/x0xx00000x

www.rsc.org/

Based on the nonlinear fluorescence enhancement, our H<sub>2</sub>O<sub>2</sub> induced supramolecular self-assembly reveals a H<sub>2</sub>O<sub>2</sub> threshold among multiple cancer and normal cells. Oxidative elimination restores an intramolecular hydrogen bond which can planarize the molecule to generate a fluorophore. The planarization enhances the intermolecular  $\pi$ - $\pi$  stacking to promote self-assembly.

Reactive oxygen species (ROS), mainly produced in mitochondria, are the normal products in oxygen metabolism.<sup>1,2</sup> ROS studies have revealed its dual biological properties: as signaling agents and as harmful molecules.<sup>3-5</sup> At the basal level with the strict regulation by redox homeostasis, ROS participate in a wide range of biological processes.<sup>6</sup> However, the dysfunction in ROS regulation, usually caused by excessive and sustained inflammation, are susceptible of the generation and exacerbation of a range of diseases including epilepsy,<sup>7</sup> Alzheimer's<sup>8</sup> and cancer.<sup>9,10</sup> In such a disease state, one common feature is the ROS over-production to exceed certain threshold.<sup>11,12</sup> Therefore, a series of molecular ROS probes with various modalities including optical,<sup>13,14</sup> <sup>13</sup>C MRI,<sup>15</sup> and PET<sup>16</sup> have been developed to observe the fluctuation of ROS.<sup>17</sup> For example, a typical hydrogen peroxide (the major ROS) fluorescent probe restores its fluorescence signal after removing the aryl boronate caging group *via* H<sub>2</sub>O<sub>2</sub> mediated oxidation.<sup>18</sup> The swift reaction allows the real time read-out of the elevated H<sub>2</sub>O<sub>2</sub> level.<sup>19,20</sup> It is worthy to mention that the stoichiometric reaction gives the signal increase *proportional* to the H<sub>2</sub>O<sub>2</sub> (or RNS) concentration. As the detection limit is always a holy grail for H<sub>2</sub>O<sub>2</sub> probes, continuous efforts focus on the amplification of the H<sub>2</sub>O<sub>2</sub> sensitivity, *e.g.* by degrading polymer backbone via single oxidation.<sup>21</sup>



**Scheme 1.** The illustration of ROS induced intracellular supramolecular self-assembly in cancer cells.

Nevertheless, since ROS intrinsically exists in all living bio-entities at a basal level, the ROS threshold is the real marker in the pathophysiologic diagnosis. Then, pushing the detection limit of ROS to an extremely low concentration is less relevant to the concern in healthcare. Instead, the capability to report the ROS threshold is critical for the judgment of normal or pathologic regimes, which has been seldom explored. A recent study has utilized a post-assembled nanoprobe with AIE luminogens to report extracellular RNS (ONOO<sup>-</sup>) at the inflammation detection window with a 20-fold enhancement in fluorescence.<sup>22</sup> However, the reason for the “silence” before the onset ONOO<sup>-</sup> concentration remains unclear. Here we developed a redox self-assembly system as a *nonlinear* reporter for H<sub>2</sub>O<sub>2</sub> (the major ROS) with a 260 times enhancement in fluorescence emission. Our molecular design has enabled fluorescent silence at basal H<sub>2</sub>O<sub>2</sub> level but a burst of increase in fluorescence intensity upon certain threshold, which is dependent on the critical assembly concentration (CAC). In addition, this redox self-assembly is applicable to profile the native intracellular redox status, thus precisely distinguish malignant cells from normal cells which is of urgent need to reveal the heterogeneity in cancer diagnosis.

<sup>1</sup>CAS Center for Excellence in Nanoscience, CAS Key Laboratory of Biomedical Effects of Nanomaterials and Nanosafety, National Center for Nanoscience and Technology Beijing 100190, China

E-mail: [gaoy@nanoctr.cn](mailto:gaoy@nanoctr.cn)

Electronic Supplementary Information (ESI) available. See DOI: 10.1039/x0xx00000x

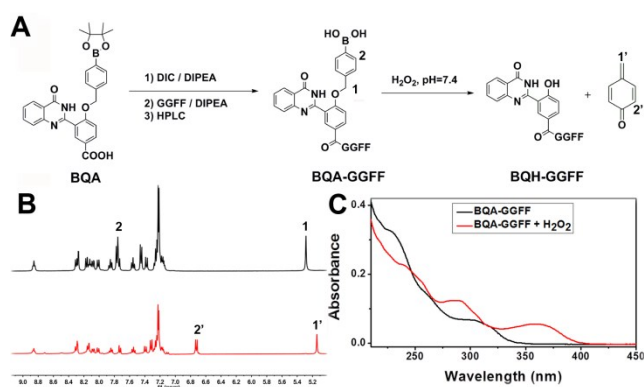


**Figure 1.** (A) The synthesis of BQA-GGFF and the generation of BQH-GGFF upon oxidation by  $\text{H}_2\text{O}_2$ . Comparison of (B)  $^1\text{H}$  NMR and (C) UV spectra of BQA-GGFF (black) and the corresponding oxidation products (red) after addition of  $\text{H}_2\text{O}_2$ .

Following the bio-inspiration strategy, such as enzymatic self-assembly,<sup>23-36</sup> we designed the redox supramolecular assembly (ROSA) using  $\text{H}_2\text{O}_2$  as the trigger to conduct the oxidation reaction and promote the intermolecular  $\pi$ - $\pi$  stacking. The synthesized assembling molecule precursor composed of a  $\text{H}_2\text{O}_2$  activatable fluorogenic BQA and a tetra peptide GGFF. BQA was a quinazolinone derivative<sup>37-39</sup> capped with a typical aryl boronate immolative linker which readily restored the critical phenyl to form intramolecular hydrogen bond upon oxidation. The formation of that intramolecular hydrogen bond was strictly correlated the generation of the fluorophore BQH which made the molecule planar. The planarization facilitated the intermolecular  $\pi$ - $\pi$  stacking to promote self-assembly.<sup>40,41</sup> Interestingly, in conjugation with GGFF, the formation of fluorophore BQH was not straightforward but dependent on the CAC. In soluble state (below CAC) the formation of fluorophore BQH was suppressed which implied the disrupted intramolecular hydrogen bond. While above CAC, the self-assembly process made the formation of the fluorophore (indication of the hydrogen bond) more favorable than its non-fluorescent form in their equilibrium. Therefore, we observed the simultaneous self-assembly and fluorescence turn-on. Although the oxidation reaction was still stoichiometric and linear, the synergistic self-assembly and fluorophore formation resulted in the nonlinear fluorescence enhancement (Scheme 1). Further incubation of BQA-GGFF with various mammalian cells revealed the selective formation of highly fluorescent assemblies inside malignant cells (Hep G2, MCF-7, PANC-1 and HeLa) instead of corresponding normal cells (L-O2, MCF-10A and HUVEC). Inductively, our study demonstrated a redox self-assembly strategy to construct intracellular fluorescent assemblies which was dependent on oxygen metabolism level. As the CAC can be easily modulated by the short peptide sequence, the strategy is expected to be applicable in other diseases with ROS threshold feature. In addition, without usual targeting moiety such as triphenylphosphine,<sup>42</sup> the assemblies could also target mitochondria which is likely due to the reaction (oxidation) based kinetic control.<sup>43</sup>

We started the study with the synthesis of the BQA moiety based on the classic synthesis of quinazolinone derivative (Scheme S1).<sup>44</sup> A sequential NHS activation and ester-amide

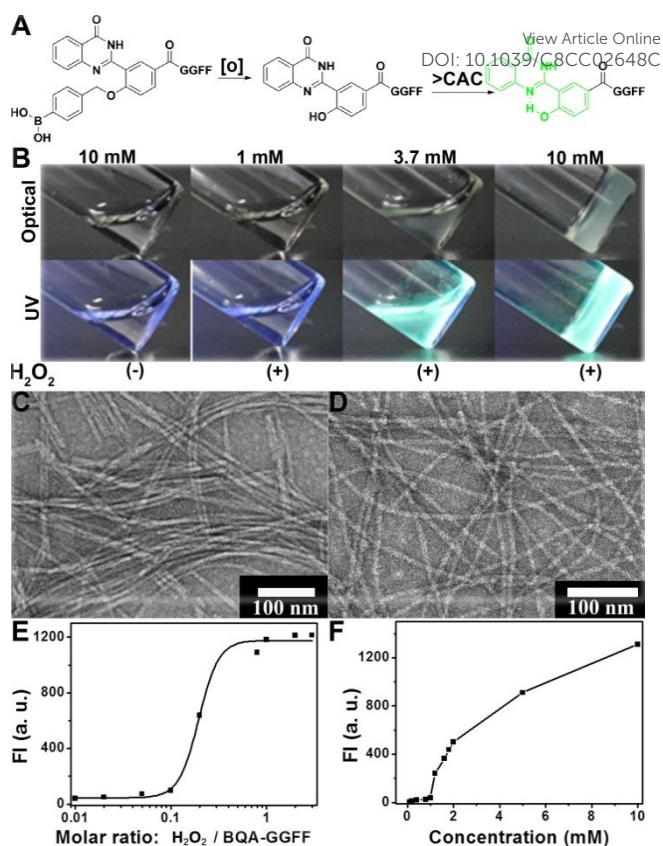


**Figure 2.** (A)  $\text{H}_2\text{O}_2$  mediated oxidation and the formation of the fluorophore upon self-assembly. (B) The determination of the critical assembly and hydrogelation concentration of BQH-GGFF in water at pH 7.4. TEM image of the assemblies of BQH-GGFF at the concentrations of (C) 2 mM and (D) 10 mM. (E) The fluorescence development (emission at 490 nm) during the titration of  $\text{H}_2\text{O}_2$  (0.01-3 eq.) into 10 mM of BQA-GGFF. (F) The fluorescence intensities (emission at 490 nm) of a series of concentrations (0.1-10 mM) of BQA-GGFF reacted to 3 eq. of  $\text{H}_2\text{O}_2$ .

exchange reaction yielded the product of BQA-peptide conjugate after HPLC purification. (Figure 1A) Then we tested the hydrogelation capability of BQA-peptides upon oxidation by  $\text{H}_2\text{O}_2$ . After screening a series of short peptides including FF, FG, GF, GG, GFF, FFG, GGFF, BQA-GGFF could perform the solution-hydrogel transition after oxidation under physiological pH and will be investigated in further studies. (Table S1)

The oxidation of arylboronic acid on BQA-GGFF initiated a 1, 6-elimination to unmask the phenol group and convert BQA to BQH. After the addition of  $\text{H}_2\text{O}_2$  into the solution of BQA-GGFF, two characteristic peaks of hydrogens (labelled 1 and 2) shifted from 5.29 ppm and 7.21 ppm to 5.14 ppm and 6.72 ppm (1' and 2'), respectively. (Figure 1B and Figure S1) Further in the UV spectra, the BQA-GGFF showed a characteristic peak at 304 nm while after oxidation the BQH-GGFF gave a red-shifted absorption peak at 356 nm. (Figure 1C) Due to the molecular structure change, the retention time of BQA-GGFF also differed from that of BQH-GGFF in HPLC traces. (Figure S2)

The self-assembly and hydrogelation depended on both CAC and the intramolecular hydrogen bond. The intramolecular hydrogen bond would planarize the whole molecule, which promotes the intermolecular interaction and assembly. The generation of BQH with phenol group provided the possibility

for the formation of intramolecular hydrogen bond but it only occurred when the concentration exceeded the CAC with the indication of fluorescence turn-on. (Figure 2A) As shown in Figure 2B, the solution of BQA-GGFF at the concentration as high as 10 mM remained non-fluorescent. When adding 3 eq. of  $H_2O_2$  into the solution of BQA-GGFF at different concentrations, the fluorescence significantly increased. Specifically, the solution remained non-fluorescent at the concentration below 1 mM but a brightly fluorescent hydrogel formed at the concentration of 10 mM with stable fluorescence emission against variant temperature or pH. (Figure S3-4) A concentration in-between (e.g. 3.7 mM) gave a fluorescent but weak hydrogel. To verify the micro morphology of the nanostructures, TEM images revealed the existence of abundant nanofibers in both weak and stable hydrogel samples, with the diameter at  $11.8 \pm 0.5$  nm and  $9.5 \pm 0.6$  nm, respectively. (Figure 2C-D) While in the 1 mM solution sample, we noticed the absence of any significant nanostructure. (Figure S5) A further rheological test confirmed the formation of a stable hydrogel. The storage modulus was around 3 kilopascal and both the storage and loss modules were frequency independent. (Figure S6-7) We determined the CAC by titrating  $H_2O_2$  into the solution of 10 mM of BQA-GGFF. With the excitation at 406nm, the solution emitted at 490nm and the intensity rose along the addition of  $H_2O_2$ . (Figure S8) Interestingly, the plot of the emission intensity vs. the amount of  $H_2O_2$  was obviously nonlinear, showing a burst increase between 0.1-0.2 eq. and a plateau with 1 eq. of  $H_2O_2$ , reaching a 260-times enhancement in emission. The burst increase indicated the CAC between 1-2 mM for BQA-GGFF. (Figure 2E) Alternatively, the trend of the emission intensities of a series of BQA-GGFF solutions at concentrations ranging from 0.1 to 10 mM after the addition of 3 eq. of  $H_2O_2$ . (Figure S9) The plot of intensity vs. BQA-GGFF concentration further indicated the CAC around 1.2 mM, which was consistent with previous determination. (Figure 2F) Such a nonlinear enhancement was attributed to the occurrence of self-assembly. At low

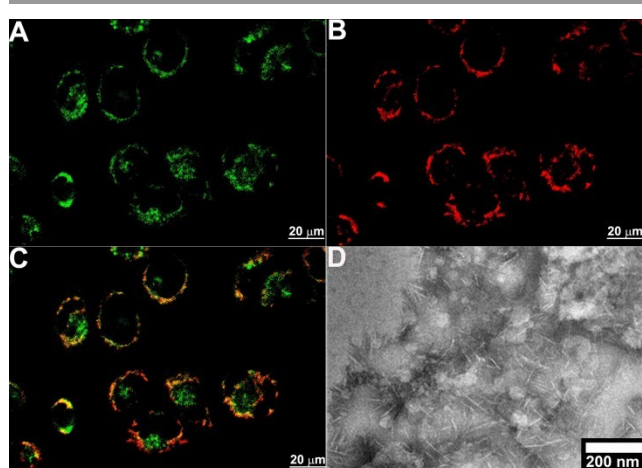


**Figure 3.** The fluorescent images of a group of HeLa cells incubated with 500  $\mu$ M BQA-GGFF and co-stained with Mito tracker. (A) The green channel of BQA-GGFF, (B) The red channel of Mito tracker and (C) The merged channels. (D) A typical TEM image showed the existence of nanofibrils in the mitochondria fraction among cellular fractions.

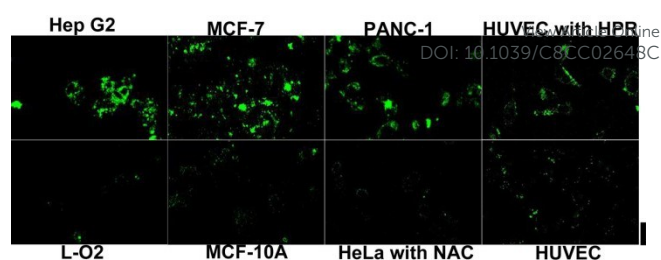


**Figure 4.** BQA-GGFF distinguishes cancer cells from normal cells. Fluorescent images of various cells incubated with 500  $\mu$ M of BQA-GGFF. Scale bar: 20  $\mu$ m.

concentration below 1 mM, BQA-GGFF was completely soluble in water without the formation of intramolecular hydrogen bond and thus remained non-fluorescent. Once the concentration was above the CAC, the self-assembly would occur with the formation of intramolecular hydrogen bond, resulting in the simultaneous fluorescence turn-on. (Figure S10)

After correlating fluorescence and self-assembly *in vitro*, we further verified if it can serve to nonlinearly detect ROS in complex biological environment such as in cancer cells.<sup>45</sup> In screening the concentration and incubation time, we found that the 500  $\mu$ M BQA-GGFF was non-toxic (Figure S11) and sufficient to form fluorescent assemblies inside HeLa cells. (Figure 3A & S12) The optimized incubation time was 8 h since the brightness faded thereafter. (Figure S13) In contrast, fluorescent assemblies were absent in HeLa cells incubated with BQA-GG which cannot self-assemble at physiological condition. (Table S1 & Figure S14) As the over-production of ROS was due to the dysfunction of mitochondria,<sup>9</sup> we expect that the formation of fluorescent assemblies are related to mitochondria. The co-staining showed the strong overlap (92.6%) between BQA-GGFF (green) and MitoTracker (red). (Figure 3C) Based on a standard fractionation procedure,<sup>46</sup> in the mito fraction we could observe the nanofibers with the diameter of  $9.1 \pm 0.9$  nm which was similar to *in vitro* one, while the nanofibers was absent in HUVEC cells. (Figure S15)

Further, we verified that the ROS-induced supramolecular self-assembly will generally form in a broad range of cancer cells instead of normal cells. (Figure 4) For the group of malignant cancer cells including Hep G2, MCF-7, and PANC-1, there were significant amount of fluorescent assemblies formed inside cells. The corresponding normal cells such as L-O2, MCF-10A, and HUVECs cells were largely dark under confocal microscope. We interpreted that the formation of fluorescent assemblies related to the ROS level which was further verified *via* the ROS attenuation. For a group of HeLa cells pre-treated with 5 mM of ROS inhibitor N-Acetyl-cysteine (NAC), no fluorescent assemblies formed. In contrast, the 3  $\mu$ M of ROS inducer 4-hydroxyphenylretinamide (HPR) treated HUVECs acquired intracellular fluorescent assemblies as many as other malignant cancer cells. A further statistical analysis of the fluorescence intensity in each individual cell by image J showed the significant difference between "malignant" and "normal" cells. The intensities for all malignant cells were above 4 while below 4 for all normal cells. (Figure S16) Therefore, the fluorescence intensity could be an empirical reference for the judgment of the malignance of individual cell.

In conclusion, we have demonstrated a redox supramolecular self-assembly triggered by H<sub>2</sub>O<sub>2</sub>. By correlating the occurrence of supramolecular self-assembly with the nonlinear fluorescence enhancement, the CAC reflects the threshold of H<sub>2</sub>O<sub>2</sub>. As this redox supramolecular self-assembly could selectively construct assemblies inside multiple malignant cell lines, this work reveals that the threshold, rather than an absolutely low level of ROS is critical in distinguishing cancer cells from normal ones. In addition to cancer, over-produced ROS also behave critical roles in pathological conditions such as inflammation and necrosis. We would expect that the redox supramolecular self-assembly will be applicable for a vast range of theranostic purposes with proper molecular design.

This work was supported by National Key R&D Program of China (2017YFA0205901), NSFC (21675036) and "Hundred Talents Project" of the Chinese Academy of Sciences for financial support.

### Conflicts of interest

There are no conflicts of interest to declare.

### Notes and references

- W. Droge, *Physiol. Rev.*, 2002, **82**, 47-95.
- M. P. Murphy, *Biochem. J.*, 2009, **417**, 1-13.
- S. G. Rhee, *Science*, 2006, **312**, 1882-1883.
- M. Giorgio, M. Trinei, E. Migliaccio and P. G. Pelicci, *Nat. Rev. Mol. Cell Bio.*, 2007, **8**, 722-728.
- D. Harman, *J Gerontol.*, 1956, **11**, 298-300.
- B. D'Autreaux and M. B. Toledano, *Nat. Rev. Mol. Cell Bio.*, 2007, **8**, 813-824.
- A. Vezzani, J. French, T. Bartfai and T. Z. Baram, *Nat. Rev. Neurol.*, 2011, **7**, 31-40.
- H. W. Querfurth and F. M. LaFerla, *N. Engl. J. Med.*, 2010, **362**, 329-344.
- K. Ishikawa, K. Takenaga, M. Akimoto, N. Koshikawa, A. Yamaguchi, H. Imanishi, K. Nakada, Y. Honma and J. Hayashi, *Science*, 2008, **320**, 661-664.
- D. Hanahan and R. A. Weinberg, *Cell.*, 2011, **144**, 646-674.
- T. Finkel, M. Serrano and M. A. Blasco, *Nature*, 2007, **448**, 767-774.
- D. Trachootham, J. Alexandre and P. Huang, *Nat. Rev. Drug Discov.*, 2009, **8**, 579-591.
- B. C. Dickinson and C. J. Chang, *J. Am. Chem. Soc.*, 2008, **130**, 9638-9639.
- N. Karton-Lifshin, E. Segal, L. Omer, M. Portnoy, R. Satchi-Fainaro and D. Shabat, *J. Am. Chem. Soc.*, 2011, **133**, 10960-10965.
- A. R. Lippert, K. R. Keshari, J. Kurhanewicz and C. J. Chang, *J. Am. Chem. Soc.*, 2011, **133**, 3776-3779.
- V. Carroll, B. W. Michel, J. Blecha, H. VanBrocklin, K. Keshari, D. Wilson and C. J. Chang, *J. Am. Chem. Soc.*, 2014, **136**, 14742-14745.
- T. F. Brewer, F. J. Garcia, C. S. Onak, K. S. Carroll and C. J. Chang, *Ann. Rev. Biochem.*, 2015, **84**, 765-790.
- V. S. Lin, B. C. Dickinson and C. J. Chang, *Methods Enzymol.*, 2013, **526**, 19-43.
- E. W. Miller, O. Tulyanthan, E. Y. Isacoff and C. J. Chang, *Nat. Chem. Biol.*, 2007, **3**, 263-267.
- A. J. Shuhendler, K. Y. Pu, L. Cui, J. P. Uetrecht and J. H. Rao, *Nat. Biotechnol.*, 2014, **32**, 373-380.
- C. D. Lux, S. Joshi-Barr, T. Nguyen, E. Mahmoud, F. Schopf, N. Fomina and A. Almutairi, *J. Am. Chem. Soc.*, 2012, **134**, 15758-15764.
- Z. G. Song, D. Mao, S. H. P. Sung, R. T. K. Kwok, J. W. Y. Lam, D. L. Kong, D. Ding and B. Z. Tang, *Adv. Mater.*, 2016, **28**, 7249-7256.
- Z. Yang, G. Liang and B. Xu, *Acc. Chem. Res.*, 2008, **41**, 315-326.
- X. W. Du, J. Zhou, J. F. Shi and B. Xu, *Chem. Rev.*, 2015, **115**, 13165-13307.
- H. M. Wang, Z. Q. Q. Feng and B. Xu, *Chem. Soc. Rev.*, 2017, **46**, 2421-2436.
- G. L. Liang, H. J. Ren and J. H. Rao, *Nat. Chem.*, 2010, **2**, 54-60.
- Y. Gao, J. F. Shi, D. Yuan and B. Xu, *Nat. Commun.*, 2012, **3**, 1033.
- D. J. Ye, A. J. Shuhendler, L. N. Cui, L. Tong, S. S. Tee, G. Tikhomirov, D. W. Felsher and J. H. Rao, *Nat. Chem.*, 2014, **6**, 519-526.
- Y. Kuang, J. F. Shi, J. Li, D. Yuan, K. A. Alberti, Q. B. Xu and B. Xu, *Angew. Chem. Int. Ed.*, 2014, **53**, 8104-8107.
- R. A. Pires, Y. M. Abul-Haija, D. S. Costa, R. Novoa-Carballal, R. L. Reis, R. V. Ulijn and I. Pashkuleva, *J. Am. Chem. Soc.*, 2015, **137**, 576-579.
- A. Tanaka, Y. Fukuoka, Y. Morimoto, T. Honjo, D. Koda, M. Goto and T. Maruyama, *J. Am. Chem. Soc.*, 2015, **137**, 770-775.
- J. Li, Y. Kuang, J. F. Shi, *et al.*, *Angew. Chem. Int. Ed.*, 2015, **54**, 13307-13311.
- D. Zhang, G. B. Qi, Y. X. Zhao, S. L. Qiao, C. Yang and H. Wang, *Adv. Mater.*, 2015, **27**, 6125-6130.
- P. Huang, Y. Gao, J. Lin, *et al.*, *ACS Nano.*, 2015, **9**, 9517-9527.
- Z. Q. Q. Feng, H. M. Wang, R. Zhou, J. Li and B. Xu, *J. Am. Chem. Soc.*, 2017, **139**, 3950-3953.
- Y. Yuan, L. Wang, W. Du, Z. L. Ding, J. Zhang, T. Han, L. N. An, H. F. Zhang and G. L. Liang, *Angew. Chem. Int. Ed.*, 2015, **54**, 9700-9704.
- J. X. Aw, Q. Shao, Y. M. Yang, T. T. Jiang, C. Y. Ang and B. G. Xing, *Chem. Asian J.*, 2010, **5**, 1317-1321.
- L. Y. Zhou, X. B. Zhang, Y. F. Lv, C. Yang, D. Q. Lu, Y. Wu, Z. Chen, Q. L. Liu and W. H. Tan, *Anal. Chem.*, 2015, **87**, 5626-5631.
- M. Gao, S. W. Li, Y. H. Lin, Y. Geng, X. Ling, L. C. Wang, A. J. Qin and B. Tang, *ACS Sensors*, 2016, **1**, 179-184.
- J. Chen and A. J. McNeil, *J. Am. Chem. Soc.*, 2008, **130**, 16496-16497.
- M. He, J. Li, S. Tan, R. Wang and Y. Zhang, *J. Am. Chem. Soc.*, 2013, **135**, 18718-18721.
- B. C. Dickinson, D. Srikun and C. J. Chang, *Curr. Opin. Chem. Biol.*, 2010, **14**, 50-56.
- J. Zhou, X. W. Du and B. Xu, *Angew. Chem. Int. Ed.*, 2016, **55**, 5770-5775.
- Z. X. Bie, G. S. Li, L. Y. Wang, Y. Lv, J. Y. Niu and S. Gao, *Tetrahedron Lett.*, 2016, **57**, 4935-4938.
- L. B. Sullivan, D. Y. Gui and M. G. V. Heiden, *Nat. Rev. Cancer*, 2016, **16**, 680-693.
- E. Dopp, U. von Recklinghausen, L. M. Hartmann, I. Stueckradt, I. Pollok, S. Rabieh, L. Hao, A. Nussler, C. Katier, A. V. Hirner and A. W. Rettenmeier, *Drug Metab. Dispos.*, 2008, **36**, 971-979.